1-2018

Cardiovascular Biomechanical Models

Ethan Kung

CARDIOVASCULAR BIOMECHANICAL MODELS

Ethan Kung, PhD
Department of Mechanical Engineering,
Department of Bioengineering,
Clemson University,
Clemson, SC, US

ABSTRACT

Computational and *in vitro* methods offer powerful means to model the cardiovascular system and investigate biomechanics related to blood flow, cardiovascular tissue, and medical devices. These models can be constructed to directly describe human anatomy and physiology, and can be more highly controlled compared to animal models. Low-order models composed of lumped-parameter elements and simplified descriptions of cardiac function can capture the global physiology, while high-order models exhibiting detailed 3D anatomy and dynamics can provide highly realistic replication of biomechanical interactions in a small region of the circulation. Multiscale models offer the freedom to capture biomechanics in different regions at the desired level of details. In this chapter we describe the fundamentals and the current state-of-the-art of model construction both in the computational and *in vitro* approaches. These models have been applied to understand the physiologic impacts of medical device implantations, predict surgical outcomes, and investigate hemodynamics in vascular diseases; we present several illustrative case studies here. Finally we examine the pros and cons of each type of models and discuss the considerations in proper model selection for a research study.

Keywords: lumped-parameter, image-based, patient-specific, CFD, *In Vitro*, multiscale

ABBREVIATIONS

LPM: lumped-parameter model
CFD: computational fluid dynamics
RCR: resistor-capacitor-resistor
VAD: ventricular assist device

INTRODUCTION

Surgical palliation of cardiovascular abnormalities and implementation of cardiovascular medical devices are intended to modify and improve patient hemodynamic parameters such as cardiac output, blood pressure, pulmonary perfusion, and blood flow patterns. Biomechanical parameters in the cardiovascular system such as 3D flow and pressure fields, as well as stress and strain in blood vessels, have direct effects on the progression of cardiovascular diseases (Caro 1971; Glagov 1988; Ku 1985; Malek 1999). The hemodynamic forces within blood vessels directly affect the biological adaptation of vessel diameters and wall thicknesses (Langille 1989; Wolinsky 1967). The design and evaluation of implantable devices require consideration of the interactions between the device and *in vivo* forces and motions. In this chapter we will examine several types of cardiovascular biomechanical models that can account for these important interactions in the investigation of cardiovascular devices and surgical procedures.

There are two inherent limitations to using animal models for studying human biomechanics: 1) the intrinsic variabilities in living organisms make highly controlled experiments difficult and 2) the physiological differences between the model animal and human make the implications of animal study results ambiguous. For these reasons, there is great motivation to employ non-living models that offer simplified, but well-controlled experiments that can be constructed based on human physiology and anatomy. Computational and *in vitro* models are two common approaches to constructing non-living biomechanical models. Models of different orders are used to capture the behavior of the cardiovascular system at different desired levels of details. Low-order models are simplified representations capable of encompassing large regions of the cardiovascular system; and high-order models can provide detailed 3D hemodynamic information for small regions of special interest.

Since the 1960s, lumped-parameter approaches have been used to construct low-order models of the circulatory system (Thiry 1976; Westerhof 2009; Westerhof 1969). While these models do not provide spatial information, they are capable of capturing complex vascular organizations and interactions, and providing realistic estimations of hemodynamics. Starting in the 1990s, the development of high-order models based on 3D medical imaging data allowed for biomechanical models to directly represent a small portion of patient-specific anatomy (Taylor 1998a; Taylor 1998b; Taylor 1999; Milner 1998; Steinman, 2002). Together, the current state-of-the-art involves combining models of different orders and constructing multiscale models to capture the relevant information of interest at the appropriate levels of details (Corsini 2013; Kung 2011b; Kung 2013; Vukicevic 2013; Schiavazzi 2015).

In this chapter, we present the computational and *in vitro* approaches to both low-order and high-order biomechanical models of the cardiovascular system. We will discuss how these models can be coupled together to construct multiscale models; we will also look at several example applications of different model configurations. Lastly we will discuss the considerations for selecting an appropriate model suitable for a research study depending on the relevant physics and the types of parameters to be investigated.

LOW-ORDER MODELS

Low-order models are greatly simplified representations of the cardiovascular system typically used to capture the systemic behaviors of the entire circulation (or a large portion of the circulation). This approach can offer the "bird's eye view" of the system where the congregated behavior of each subcomponent is approximated without great amounts of detail. A very common type of low-order model for the cardiovascular system is the lumped-parameter model (LPM). In this approach, aspects of the cardiovascular system are represented by components analogical to electrical circuit elements. This type of model does not contain spatial information other than the structure of the vascular network represented as the corresponding circuit element organization in the model. Another type of cardiovascular low-order model is one that solves the 1D equations of blood flow (Hughes and Lubliner, 1973). This approach offers spatial information along a single dimension (down the length of blood vessels), and is a slightly more complex and computationally expensive type of low-order model. In this chapter, we will focus on the lumped-parameter approach to the low-order model.

In the vascular system, blood is driven through a vascular bed by arterial blood pressure. The vascular bed is typically considered passive in the sense that it does not generate pressure. The underlying physics governing the blood flow characteristics in a passive vascular bed can be modeled via 3 types of basic elements in the LPM: resistance, capacitance,

and inductance. The resistance element describes the viscous dissipation of pressure energy as blood flows through vasculature. The compliance of blood vessels (mostly in large vessels) is modeled by the capacitance element in the LPM, which captures the effects of blood vessel elasticity damping pressure and flow pulsations. Lastly, inductance elements are used in the LPM to describe how the momentum of blood resists changes in flow. This aspect of blood flow is especially important for accurately modeling hemodynamics in regions close to the heart (i.e., flow through the aortic valve, in the abdominal aorta, etc) where the blood flow pulsation is significant. The capacitance and inductance are non-dissipative elements.

The active components in the LPM generate pressures to drive blood through the passive vascular beds. The main active component is the heart itself; the driving pressure generated by the heart is almost always included in an LPM. Pressures generated by other active components are selectively included in each specific model depending on their relative importance to the topic being investigated. These can include respiration, muscle pumps, and medical devices such as blood pumps.

Computational Representation

Passive Components

The viscous flow resistance is modeled by the equation $P = QR$, where Q is the volumetric flow rate through the resistance, R is the resistance value, and P is the pressure drop across the resistance. In healthy situations, blood flow is laminar in most of the cardiovascular system. Small arterioles with little compliance (and thus little change in diameter over a cardiac cycle) contribute to most of vascular resistance. According to Poiseuille's solution for laminar flow in a tube, the viscous resistance of blood vessels is therefore relatively constant across the cardiac cycle at a given physiologic state. The viscous flow resistance in non-laminar flow regions, such as across heart valves or surgical shunts, are typically represented as flow-dependent resistances. The mathematical relationship between the flow and pressure drop in these elements is typically derived empirically (Migliavacca 2000).

Capacitance is modeled by the equation $Q = C\, dP/dt$, where C is the capacitance value, dP/dt is the time rate of change of the pressure across the capacitor, and Q is the volumetric flow rate into the capacitor. This equation describes the physical scenario where flow into a capacitor "charges up" the capacitor, much like how the internal pressure of an elastic balloon increases when fluid is pumped into the balloon.

Inductance is modeled by the equation $P = L\, dQ/dt$, where L is the inductance value, dQ/dt is the time rate of change of the volumetric flow rate through the inductor, and P is the pressure across the inductor. This relationship stems from Newton's second law and describes the physical scenario where a change in volumetric flow rate (acceleration) requires a pressure difference across the inductor (i.e., force applied to the fluid). A summary of the aforementioned passive components is provided in Figure 1.

Element	Symbol	Computational Model	Experimental Model	
Resistance (models viscous dissipation)	-\/\/\/\-	P = Q R		Parallel glass capillary tubes
Capacitance (models vessel compliance)	—⊣⊢—	Q = C dP/dt		Trapped air pocket
Inductance (models blood momentum)	⌁ℓℓℓℓ⌁	P = L dQ/dt		Any tubing segment (parasitic)

Figure 1. Summary of common passive elements in the lumped-parameter model.

Heart Models

There are two common types of heart models for the computational LPM: the elastance function model and the active-passive function model. The first approach utilizes the normalized elastance function to model the ventricle. The elastance "*E*" is defined as the ratio between the pressure and relative volume inside a ventricle, and by the equation *P=E(t) (V-Vo)*, where *E(t)* is the time-varying elastance, *V* is the blood volume inside the ventricle, *Vo* is the ventricle's reference volume, and *P* is the blood pressure in the ventricle. Conceptually, the elastance describes the "stiffness" of a ventricle at any point in time as it contracts and relaxes. The justification for using the normalized elastance function to model the ventricle is based on previous findings that the shape of the normalized (with respect to amplitude and timing of the peak) elastance waveform is relatively constant across people, and independent of ventricular load, contractile state, and various cardiac diseases (Suga 1973). Since the physiologic basis for the elastance function model is based on studies of the ventricle, this approach is typically not used for modeling the atria. In the implementation workflow, each elastance function model begins with the normalized elastance function (Figure 2a). This function is then "de-normalized" for each specific model simulation. The de-normalization involves stretching or shrinking the function in the x-axis according to the specific heart rate and ventricular activation to be simulated, scaling the function amplitude in the y-axis according to the contractility to be modeled, and offsetting the function in the y-axis to describe the appropriate passive filling characteristics of the ventricle (Kung 2014).
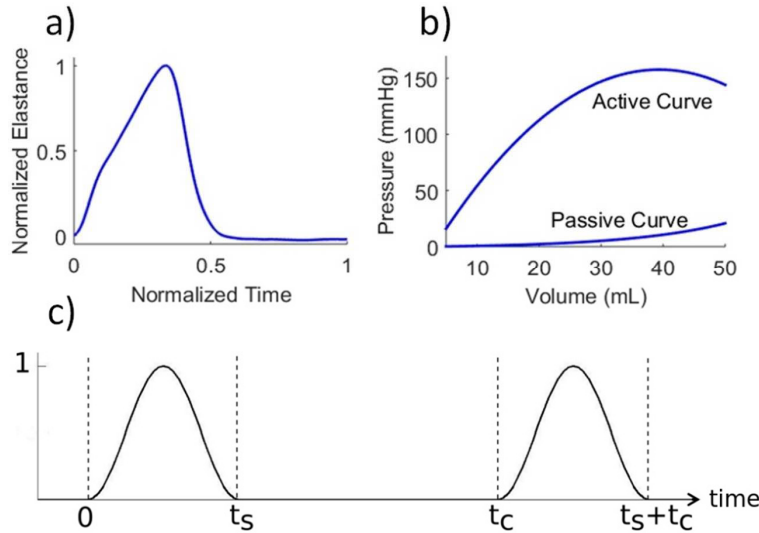

Figure 2. a) The normalized elastance function for modeling the ventricle b) An example active and passive curve for modeling a heart chamber (the ventricle of a pediatric patient is represented in this particular example) c) An example activation function to describe the cardiac contraction of each heartbeat. "tc" is the cardiac period and "ts" is the systolic length.

The active-passive function approach can be used to model both the atrium and ventricle. In the active-passive function model, two pressure-volume relationships (Figure 2b) are used to describe the active and passive behaviors of the heart chamber. The passive curve is defined based on the elastic properties of the chamber during relaxation, and the active curve is defined based on contractile characteristics. An activation function (Figure 2c) is used to describe the timing and duration of active contraction. Different shapes may be chosen for these curves depending on the design of the specific heart model. The pressure inside the heart chamber is then defined as *P=A*P_{act} + P_{pas}*, where *A*, *P_{act}*, and *P_{pas}* is the value of the activation function, active pressure, and passive pressure, respectively (Corsini 2013). Note that *A* is a function of time, and *P_{act}* and *P_{pas}* are functions of the heart chamber volume.

There are advantages and disadvantages to these two different heart modeling approaches. The elastance function approach is empirically-based; the normalized elastance function already encapsulates the congregated underlying mechanisms that result in the observed behavior of the ventricle. This model requires few parameters to be tuned for each modeling scenario, but only offers a somewhat "black box" approach to modeling the heart. The active-passive approach

mathematically describes the underlying properties of heart tissue and contraction characteristics, and offers a lower-level mechanistic approach to capturing heart function. It requires the tuning of more parameters, each needing to be set appropriately in order for the model to accurately describe the specific heart to be simulated.

Other Active Components

Mathematical descriptions of other active components driving blood flow can be constructed and implemented into the computational LPM. Like the heart model, active components are generally implemented as pressure sources. The specific mathematical constructions to describe these components can vary greatly and the discussion is beyond the scope of this chapter. Common active components that are modeled besides the heart include respiration (Kung 2014; Baretta 2012) and ventricular assist devices (Giridharan 2002; Pekkan 2005; Schmidt 2016). Interested readers are encouraged to refer to the cited literature for further details.

Example Implementation

Here we present a simple example to illustrate how to use the various components discussed to perform calculations of pressure, flow, and volumes in a computational LPM. In this exercise we use an active-passive function model to describe an atrium, an elastance function model to describe a ventricle, and a few passive components to describe a simplified vascular bed. Note that the two ideal diodes included in this LPM represent heart valves and allow uni-directional flow with no added resistance (Figure 3).

Assume that based on atrial and ventricular characteristics, we have already defined $E(t)$, $P_{act}(Va)$, $P_{pas}(Va)$, and $A(t)$, which are the de-normalized elastance function of the ventricle, the atrial active and passive pressures as functions of atrial volume, and the activation function of the atrium, respectively. Assume that based on the scenario to be modeled, we have also already determined the resistance, capacitance, and inductance component values, the initial values of differential variables, and the ventricular reference volume "Vo." The resulting system of equations describing this LPM is then:

$$Pv = E(t)(Vv - Vo) \qquad \text{(Eqn 12.1)}$$

$$Pa = A(t)P_{act}(Va) + P_{pas}(Va) \qquad \text{(Eqn 12.2)}$$

$$Q_{av} = \begin{cases} \frac{Pa-Pv}{R2} \ for \ Pa \geq Pv \\ 0 \ for \ Pv > Pa \end{cases} \qquad \text{(Eqn 12.3)}$$

$$\frac{dQ_L}{dt} = \begin{cases} 0 \ for \ Q_L \leq 0 \ and \ Pc > Pv \\ \frac{Pv-Pc}{L} \ else \end{cases} \qquad \text{(Eqn 12.4)}$$

$$\frac{dPc}{dt} = \frac{Q_L - (\frac{Pc-Pa}{R1})}{C} \qquad \text{(Eqn 12.5)}$$

$$\frac{dVa}{dt} = \frac{Pc-Pa}{R1} - Q_{av} \qquad \text{(Eqn 12.6)}$$

$$\frac{dVv}{dt} = Q_{av} - Q_L \qquad \text{(Eqn 12.7)}$$

This system of equations can be solved using a numerical time-stepping scheme, such as the 4th order Runge-Kutta method.
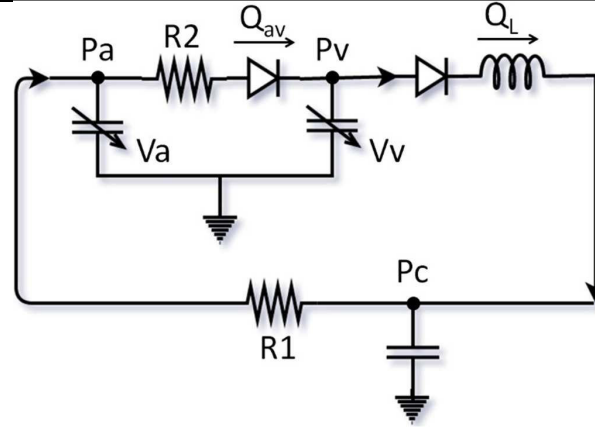
Figure 3. Schematic of the example LPM. "Va" and "Vv" are the atrial and ventricular volumes, respectively.

In Vitro Representation

Passive Component: Resistance

According to the Poisuille solution, the viscous resistance of a flow conduit is a function of only the fluid property and the geometry of the conduit as expressed by equation 12.8. Note that this solution is only valid for laminar flow; in the turbulent flow regime, the resistance is a function of also the flow rate. Due to the fact that blood flow is laminar in the large number of parallel small blood vessels, under normal physiologic conditions the viscous resistance of a vascular bed behaves similar to an ideal resistor that is not a function of flow rate. In order to replicate this vascular resistance behavior, an *in vitro* resistance component should be constructed using a large number of parallel small channels. This is supported by examining the relationship $R \propto N^{3/2} \, Re \, / \, Q$ where R is the overall resistance of a resistor component, N is the number of parallel channels used to create the resistor, Re is the Reynolds number in each individual channel, and Q is the total flow rate through the resistor (Kung 2011). For a given resistance, in order to accommodate high enough (physiologic) flow rates while maintaining Re in the laminar flow regime, a large number of parallel channels should be used (Figure 4). A practical method to construct such a flow resistance component is by placing a number of glass capillary tubes in parallel inside a larger conduit as shown in Figure 1 (Kung 2011). The following equations for calculating the resistance value "R" and maximum laminar flow rate "Q_{max}"of the resistance component are useful for its design and construction:

$$R = \frac{8 \, \mu \, l}{N \, \pi \, r^4} \qquad\qquad\qquad\qquad\qquad \text{(Eqn 12.8)}$$

$$Q_{max} = 1050 \, \pi \, \mu \, r \, N \, / \, \rho \qquad\qquad\qquad\qquad \text{(Eqn 12.9)}$$

μ and ρ are the dynamic viscosity and density of the working fluid. *l, r,* and *N* are the length, inner radius, and total number of capillary tubes.

Alternatively, many studies choose to use a simple partially closed ball valve to create flow resistance in an experiment (Figliola 2010; Vukicevic 2013; Khoiy 2016; Timms 2011). This approach results in a resistance that is a direct function of flow rate (Figure 5) (Kung 2011). In experiments where the flow is fairly constant, the simple ball valve resistor may provide a good approximation of the desired resistance. In highly pulsatile flow scenarios, the approximation begins to deteriorate. While the ball valve flow resistor is very simple to construct, it is difficult to tune. Very small adjustments of the valve closure can result in significant changes in the resulting flow resistance. When employing a ball valve resistor in an experiment, it is important to completely avoid physical perturbation of the valve after tuning. Depending on the specific topic of study, the ball valve resistor may be an appropriate option to quickly provide a desired mean resistance.
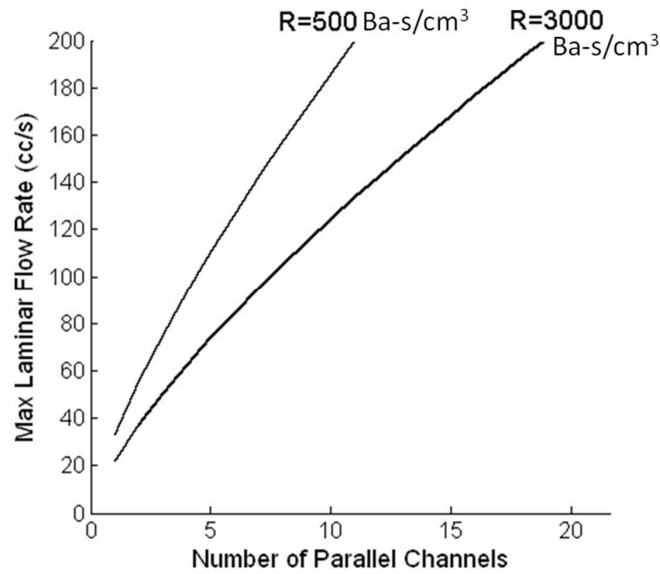
Figure 4. Maximum laminar flow rate versus number of parallel channels for the resistance component. In order to accommodate higher flow rates, a flow resistor needs to be constructed from an increasing number of parallel channels.
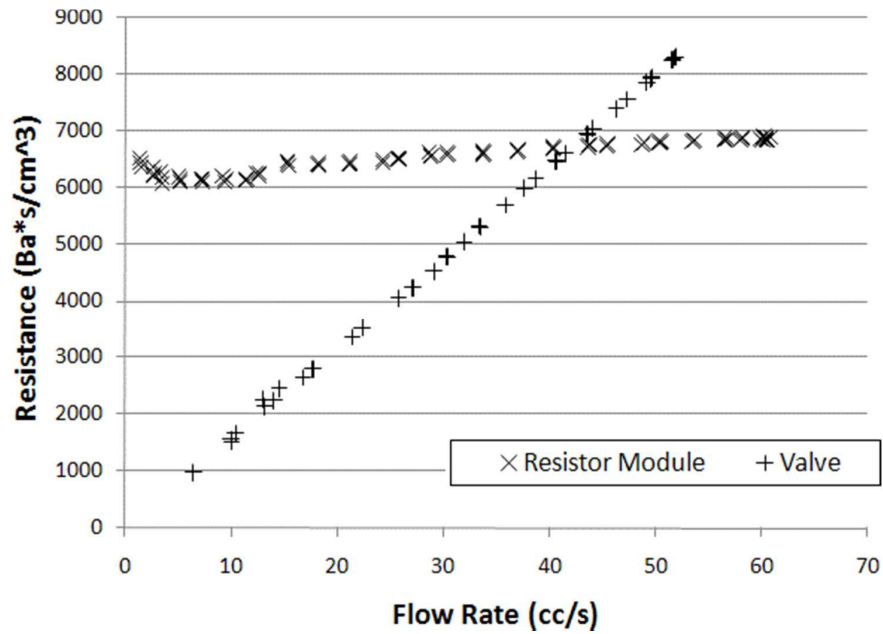

Figure 5. Resistance characteristics of a resistance component made from parallel capillary tubes, versus one made from a partially closed ball valve.

Passive Component: Capacitance

The most common method for constructing a flow capacitance is to use a chamber that traps a pocket of air, where liquid entering the chamber would compress the air pocket (Figure 1). By combining the mathematical definition of the capacitance and Boyle's law, we obtain that the capacitance of an air pocket due to compression is $C_c = V/P$, where V is the volume of the air and P is the absolute pressure of the air. For small perturbations in the air volume and pressure, the capacitance value stays fairly constant. Another contribution of capacitance that is a byproduct of the use of such a chamber is the changing height of the liquid-air interface as liquid enters and leaves the chamber. Using hydrostatic calculations we obtain that this capacitance is $C_h = A / \rho g$, where A is the horizontal cross-sectional area of the chamber, ρ is the density of the liquid, and g is gravity. C_c and C_h are two capacitances in series resulting from this setup. C_h is typically much larger than C_c and thus can be neglected with the two capacitances being in series. In the case where a very large capacitance is desired, a chamber that is open to the atmosphere can be used. In such a construction the capacitance is described by C_h alone (Kung 2011).

Passive Component: Inductance

The flow inductance describes how the acceleration of fluid results in a force which manifests as a pressure differential. Due to the fluid mass in flow conduits, the inductance is often a parasitic parameter in an *in vitro* experiment. The inductance "L" of a flow conduit can be calculated by $L = \rho l / A$ where l is the length and A the cross-sectional area of the conduit (Kung 2011). Inductance can be added to a flow system by simply putting in sections of long tubing. However, it is uncommon to insert tubing for the sole purpose of adding inductance, since the inherent inductance of existing connection tubing required in a flow system is often already sufficient or more than the desired vascular inductance to be modeled.

Active Components

The fluid flow in an *in vitro* experiment is typically driven using programmable flow pump. Commercial devices such as the 'Harvard pump' (Harvard Apparatus, Holliston. MA, USA) and the 'SuperPump' (Vivitro Labs, Victoria, BC, Canada) operate on a piston pump principle and are capable of generating outputs that resemble the flow through the aortic valve (containing regions of zero flow). The output of this type of pumps must contain a zero flow region due to the necessity for the piston cylinder to refill in each cardiac cycle. These pumps are relatively simple and inexpensive, and are ideal for *in vitro* experiments replicating flow conditions in regions near the heart. In order to create flow conditions corresponding to those at specific vascular regions further away from the heart, extensive downstream vascular simulator (i.e., an *in vitro* LPM) may be required to provide the necessary impedances (Groves 2014; Pahlevan 2013). The proper construction and tuning of the vascular simulator may be taxing.

A more sophisticated type of programmable flow pump utilizes a gear pump together with a stepper or servo motor to create output flow waveforms of an arbitrary shape. Custom built devices (Mechoor 2016) or commercial devices such as the 'CardioFlow' (Shelley Medical Imaging Technologies, London, ON, Canada) can generate flow waveforms precisely corresponding to those at specific anatomic locations. A feedback mechanism that adjusts motor input signal based on the actual flow output (Mechoor 2016) can be used to correct any errors in the output flow waveform due to varying downstream loading conditions. This type of programmable flow pump is the best option for re-creating precise flow waveform shapes without the need for complicated vascular simulator setup and tuning.

A programmable flow pump together with real-time pressure measurement feedback can construct an *in vitro* active component that approximates the Frank-Starling behavior of the heart, albeit without highly realistic end-systolic and end-diastolic pressure-volume characteristics and preload sensitivities (Baloa 2001; Gregory 2011; Gwak 2005; Timms 2011; Pantalos 2004; Ferrari 1998).

In the human body, the movement of the diaphragm due to respiration leads to dynamically changing pressures inside the thoracic and abdominal cavities, which then act on the blood vessels in those cavities to affect blood flow. An *in vitro* setup can capture this effect by applying an external pressure, typically by pneumatics, to flexible tubing that represent large blood vessels in those cavities.

Constructing the LPM

A vascular bed can typically be represented as a resistor-capacitor-resistor (RCR) block (Figure 6), with the proximal resistor *"Rp"* representing the combined resistance of the larger arteries, the capacitor *"C"* representing the combined compliance of the elastic vessels, and the distal resistor *"Rd"* representing the combined resistance of the arterioles and capillaries of the vascular bed. An additional capacitor and resistor are sometimes added to the RCR block to describe the venous compliance and resistance. RCR blocks representing different vascular beds are then organized together to represent the circulation to be modeled (Figure 7). Based on the goals of a specific research study and the particular regions of interest, the researcher must determine the appropriate amount of details when constructing different parts of the LPM. Inductors should be added to points of the LPM where flow is highly pulsatile. Active components such as the atria, ventricles, and respiration should be added as pertinent to the study.

Once the structure of the LPM is determined, the component values and parameters of the LPM are often tuned based on clinical data acquired from the patients to be modeled. The averaged pressure drop and the flow across a vascular network together determine the total resistance of the network. The ratio of the proximal to the distal resistance, as well as the value of the capacitance both affect the shape of the flow and pressure waveforms. For example, given a specific inflow waveform to a vascular block, increasing the capacitor component value or decreasing the ratio of the proximal to distal resistance will result in decreased pressure waveform amplitude at the inlet of the block. An iterative process is often used to tune the values of the LPM components, as well as sometimes the structure of the LPM circuit, until the LPM produces hemodynamic conditions that match the corresponding clinical measurements.
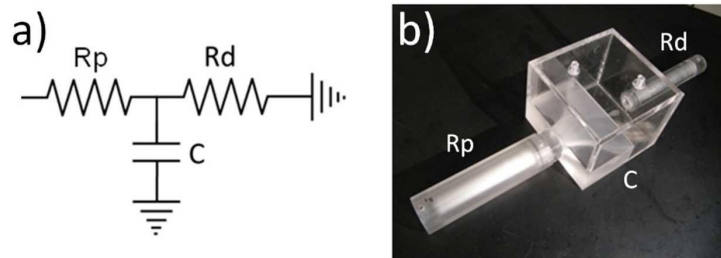

Figure 6. Basic lumped-parameter representation of a vascular bed using the resistor-capacitor- resistor block. a) Symbolic representation; b) *In vitro* physical module.
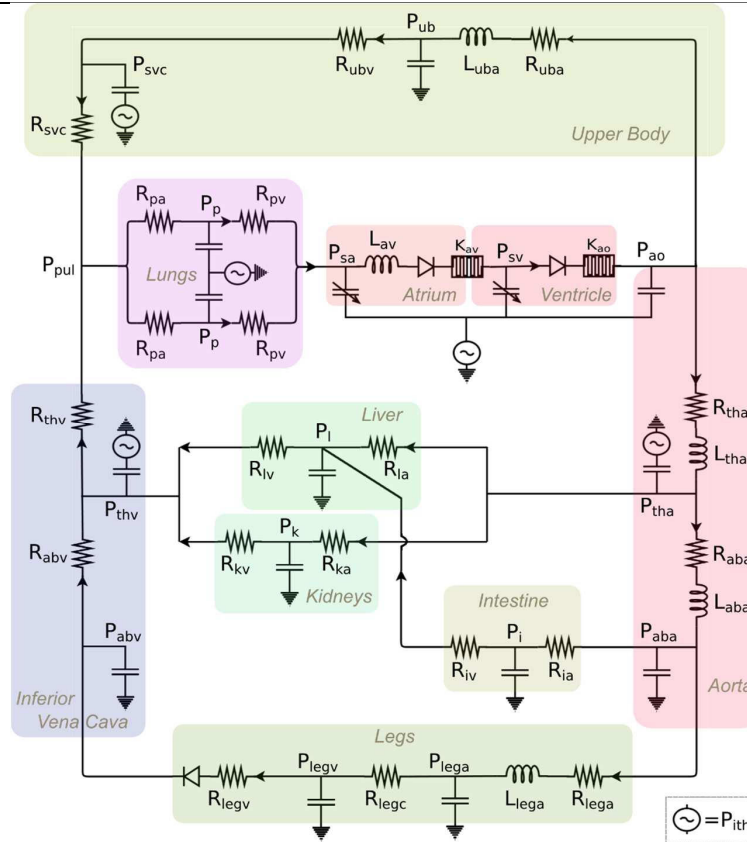
Figure 7. An example LPM describing the single-ventricle circulation. Pith represents the thoracic pressure. (Kung 2014).
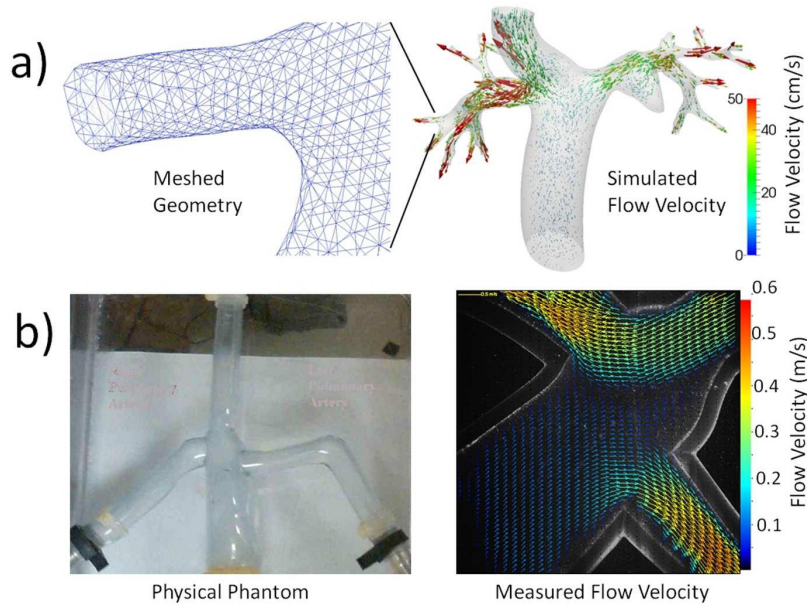

Figure 8. Analysis of blood flow patterns using a a) computational; and b) experimental[1] high-order model.

---

[1] Courtesy Richard Figliola.

HIGH-ORDER MODELS

High-order models are capable of capturing detailed 3D dynamics that are dependent on anatomy and geometry (Figure 8). They are useful in situations where the details of these parameters have global effects, or are important to the topic of interest. For example, the design of the propeller in a blood pump or the proper closure of a heart valve has important impacts to the global hemodynamics (such as cardiac output and blood pressure). The blood flow pattern in an aneurysm revealing local areas of recirculation or low vessel wall shear stress may suggest thrombotic risks or biological responses that contribute to aneurysm enlargement. For these types of studies it is often necessary to use high-order models to capture the relevant dynamics.

The scope of high-order models is typically limited to small regions of the circulation, since the complexity and cost of high-order models make it currently impractical to model the entire circulation with them. 3D medical imaging data such as those from computed tomography or magnetic resonance imaging provide the geometrical basis for model construction. 3D segmentation based on image intensity and 2D segmentation along blood vessel centerlines are common methods for reconstructing high-order models that reflect patient-specific anatomy (Soler 2001; Les 2010). Using patient-specific high-order models, different surgical procedures can be attempted and evaluated via computational simulations or *in vitro* experiments. Models of vasculature with deformable walls are also capable of capturing important fluid-structure interactions in the cardiovascular system. Currently, one of the main challenges with utilizing deformable-wall models is the difficulty in prescribing relevant tissue properties, as this information is difficult to obtain from patients non-invasively.

Computational Representation

In a computational high-order model, the relevant geometry is discretized into a large number of entities (elements or control volumes) (Krause 1985; Peskin, 1972) using meshing software. Blood flow velocity and pressure are then computed using finite volume or finite element methods by solving the well-known mass conservation and incompressible Navier-Stokes equations. Newtonian fluid assumption is widely accepted for modeling hemodynamics in large blood vessels (Gijsen 1999). Non-Newtonian shear thinning behavior of blood needs to be considered in modeling scenarios such as capillary flow and flow near blood vessel walls. High-performance parallel computing and significant storage capacity are typically required for running high-order computational models.

To incorporate the effects of blood vessel wall deformation, the coupled momentum method (Figueroa 2006) was developed to be a computationally inexpensive method for capturing fluid-structure interactions. In this approach the blood vessel wall motion is prescribed as a velocity boundary condition to the fluid domain, while the fluid mesh remains fixed. This method is suitable in scenarios where the vessel deformation is small, and has been experimentally validated to produce reasonably accurate results for vessel-wall strains up to ~10% (Kung 2011a). For cases where the geometric deformation is large, the Arbitrary Lagrangian-Eulerian method (Long 2012; Bazilevs 2010) is often employed. In this method, the fluid mesh is moved in each computation step based on vessel wall motion and reconstructed when the geometrical deformation becomes large, resulting in a drastic increase in computational expense.

An alternative approach that does not require mesh reconstruction during large geometric deformation is the immersed boundary method (Peskin 1972; Zheng 2012). In this method the entire fluid domain is represented as a fixed Eulerian mesh with an arbitrary mobile boundary that represents the fluid-structure interface. This approach has been an active area of research especially for simulating heart valves (Griffith 2012; Wu 2016; Watton 2007; Borazjani 2013). One of the main limitations of the immersed boundary method is the lack of mesh density control with respect to the specific geometry to be modeled and thus difficulty in obtaining accurate shear stresses near fluid-structure interfaces.

There are various computational approaches for capturing the fluid-structure interaction involving the active myocardial wall motion. These can include the direct prescription of cardiac wall motion based on time-resolved imaging data (Lee 2013), and electromechanical models that simulate cardiac motion based on myocardial fiber orientation and activation (Trayanova 2011; Bayer 2012).

In Vitro Representation

High-order *in vitro* models typically involve a physical replica of the anatomy, geometry, or medical device to be investigated. A physical model of the anatomy with which flow experiments can be performed is referred to as a "phantom." Stereolithography (3D-printing) is a popular method for physically reconstructing patient specific anatomy. Commercial materials such as Somos® WaterShed plastic provide suitable options for 3D-printing rigid phantoms (Kung 2011b). However, there is currently no suitable material option for 3D-printing compliant phantoms with elastic properties that mimic real blood vessels. Rubber-like stereolithography materials such as TangoPlus (Stratasys Inc.) produce homogeneous compliant phantoms that are more visco-elastic than real vascular tissue. Phantoms made with silicon currently have the most realistic compliant properties, but cannot be 3D-printed. Highly uniform and sub-millimeter wall thickness is often desired in a compliant silicon vascular phantom. This can be achieved via a silicon dipping process for a phantom with trivial geometry (Kung 2011a). More complex phantom geometries need to be constructed using a silicon casting process involving an inner and outer mold; however, uniform and sub-millimeter wall thickness is difficult to achieve this way.

The selection of phantom material needs to account for compatibility with the desired mode of *in vitro* measurements. For example, phantoms for flow experiments intended in a particle imaging velocimetry study must have similar index of refraction as the working fluid. Studies employing ultrasound imaging should use phantoms with minimal acoustic attenuation and reflection. Phantoms used in magnetic resonance imaging studies must be made with materials that do not contain metal traces to avoid imaging artifacts.

A popular working fluid for *in vitro* models is 40% glycerol solution. This fluid possesses density and viscosity that are similar to those of blood and hence exhibits realistic fluid dynamic behaviors.

Coupled Multiscale Models

While the isolated use of a low-order model can have practical utilities (Schmidt 2016, Kung 2015), a high-order model is rarely used on its own since it only captures a very small region of the cardiovascular system. Much of the dynamics in a high-order model is determined by its boundary conditions. We can see from the computational simulation results in Figure 9 that the same geometric model with different outlet boundary condition prescriptions exhibits completely different pressure and flow behaviors. Proper boundary condition prescriptions in high-order models are essential for generating the correct flow split between multiple outlets and the proper pressure waveforms for producing accurate tissue movements in deformable models. In order to obtain realistic boundary conditions, a high-order model can be coupled to a low-order model, forming a multiscale model containing different domains. Figure 10 illustrates example multiscale models where a high-order anatomic model is coupled to a low-order LPM in order to reproduce local hemodynamics in a specific anatomic region within the context of the larger circulation.

In a multiscale model, the flow and pressure in each of the domains are coupled in a way such that they directly affect those in the other. The technical implementation of this coupling in the computational model involves passing flow and pressure information between the high-order and low-order models at each simulation time step. At each interface between the two domains, boundary condition is prescribed to the high-order model as either the Neumann or Dirichlet condition. The Neumann boundary condition is suitable when the most adjacent differential element in the low-order model near the interface is a capacitance. In this type of boundary condition, the low-order model provides pressure information to the high-order model, and the high-order model provides flow rate information to the low-order model. The Dirichlet boundary condition is suitable when the most adjacent differential element in the low-order model near the interface is an inductance. In this case, the low-order and high-order model provides flow and pressure information to the other, respectively. In an *in vitro* multiscale model, the coupling between the high and low order models can occur simply via direct physical connections (Figure 10b).

A coupled multiscale model can be categorized as either open-loop or closed-loop. The differentiation lies in whether the model is designed in a way such that the dynamic response of the heart is reflected. An open-loop model typically prescribes a fixed pressure or flow waveform as the active driver of the system, where a closed-loop model contains a heart model actively responding to factors such as preload and afterload. The open-loop model is simple to set up and suitable for studies focusing on the isolated dynamics of the high-order model. However, when the global physiological response is an important aspect of a study, the closed-loop model should be used.
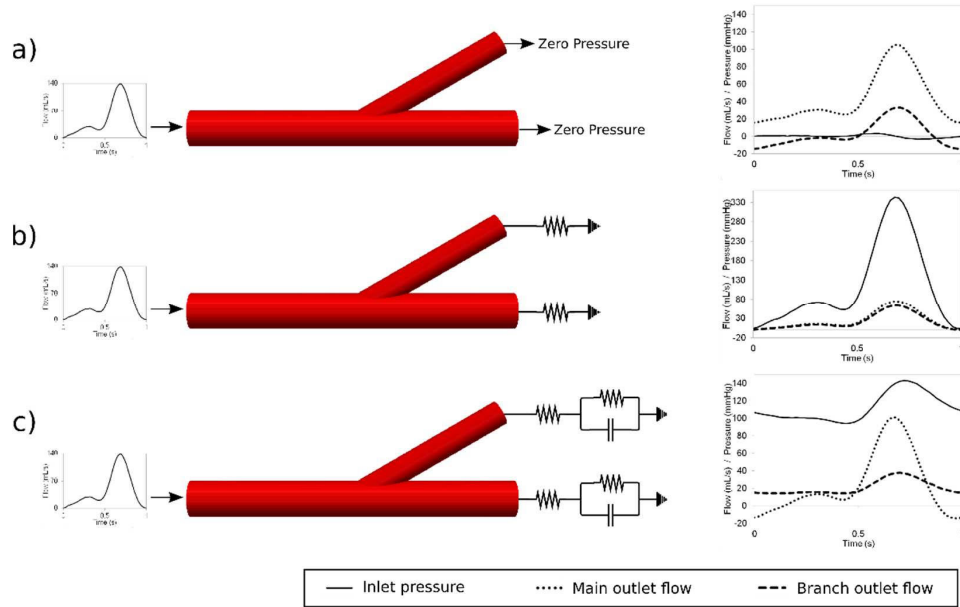
Figure 9. (a) Zero pressure; (b) resistance; and (c) RCR outlet boundary conditions prescribed to the same geometric model show that results in the high-order model are directly dependent on the prescribed boundary conditions. (Marsden 2015).
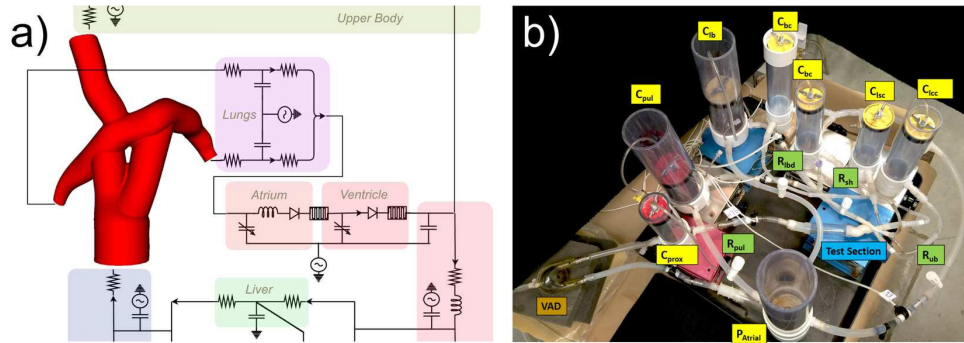

Figure 10. Example multiscale models of the single-ventricle circulation: a) Computational model of the stage 3 circulation with a high-order model representing the Fontan junction; and b) *In vitro* model of the stage 1 circulation with a high-order model representing the aortic arch and pulmonary shunt[a].

EXAMPLE CASE STUDIES:

Ventricular Assist Device Implementation in Single Ventricle Infants: Low-Order Closed-Loop Computational Model

In this case study we examine the use of a low-order closed-loop computational model to investigate the physiologic impacts of ventricular assist device (VAD) implementation in single ventricle infants (Schmidt 2016). We will see how the model delineates mechanisms behind performance differences often observed clinically between steady and pulsatile VADs.

A VAD can be used as mechanical support in heart failure patients either as bridge-to-transplant, bridge-to-recovery, or destination therapy. VADs are used in various types of circulations including single ventricle circulations (Calvaruso 2007; Cardarelli 2009; Chu 2007) and normal bi-ventricular circulations (Hetzer 2006; Stiller 2003; Adachi 2011). The two main categories of these devices are the pulsatile or continuous flow VAD. A Pulsatile flow VAD (such as the Berlin Heart) drives blood via a pneumatically actuated membrane and one-way valves located at the inlet and outlet of the blood chamber, emulating the heart's distinct phases of diastole and systole. Some evidences suggest that pulsatile flow VAD may promote better ventricular unloading and more natural physiology (Cheng 2014; Drews 2008; Klotz 2004). Continuous flow VADs use spinning propellers to produce a pressure rise (Moazami 2013) and often have better reliability and smaller size, providing reduced risk of infection, bleeding, trauma, and thrombus (Cheng 2014; Drews 2008; Feller 2007; Kato 2011).

In this case study we use a closed-loop computational LPM (Figure 11) to investigate the physiologic response of stage 1 single ventricle patients to pulsatile and continuous flow VADs, and to identify mechanistic explanations for the differences in physiologic outcomes. Clinical data from six stage 1 single ventricle patients are used to tune the LPM to create six models each describing a unique patient. Ventricular contractility in each LPM is then diminished to simulate a heart failure condition. The HeartWare VAD and the Berlin Heart EXCOR VAD are each implemented in the LPM to describe the continuous and pulsatile VAD scenario, respectively. As the VAD attempts to draw blood from the ventricle, a negative ventricular pressure may result which could lead to ventricular tissue being drawn into the cannula and ventricular collapse (Salamonsen 2015). As part of the VAD implementation in the LPM, a ventricular suction equation is developed and incorporated to describe the suction resistance "R_{SUC}" due to ventricular collapse, thereby impeding VAD flow (Schmidt 2016).

The results of this modeling study show that the continuous VAD is capable of providing significantly higher cardiac output in all of the six patient physiologies examined (Table 11.1). Closer examination of the blood volume inside the pulsatile VAD reveals the underlying mechanism responsible for this difference. For the pulsatile VAD, cardiac output increases are achieved by means of increasing device heart rate or device size (i.e., maximum stroke volume). However, if a large pulsatile VAD is implemented in a stage 1 single ventricle patient, who typically is a small infant, ventricular suction tends to occur and the device is unable to fill completely during diastole as its pump rate increases (Figure 12). The decreased stroke volume at higher pump rates results in the inability to augment cardiac output.
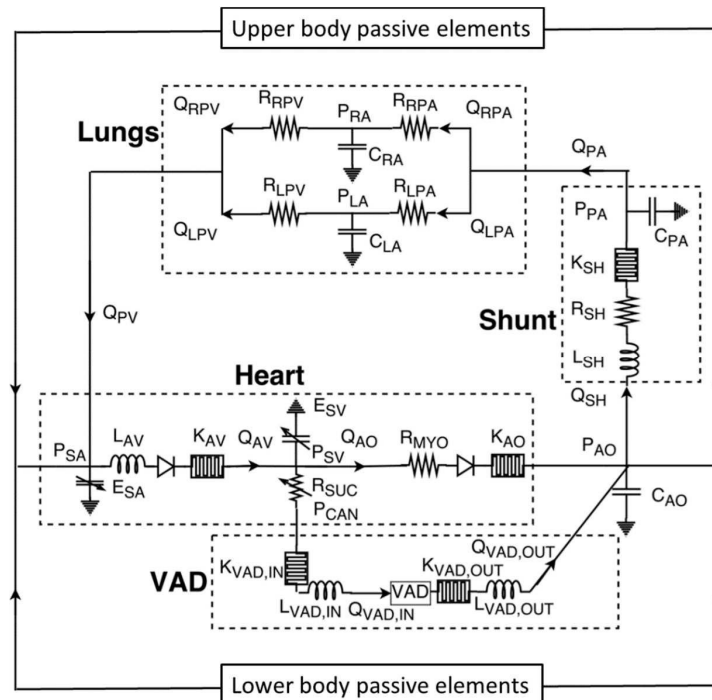

Figure 11. A low-order closed-loop computational model describing a ventricular assist device implemented in the stage 1 single-ventricle circulation.
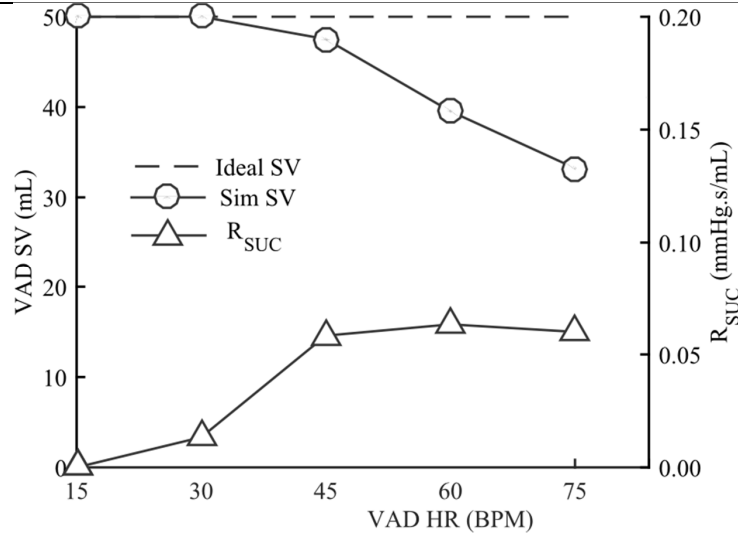
Figure 12. Stroke volume (SV) and suction resistance (R_{SUC}) versus VAD heart rate (HR) for the 50 mL Berlin Heart. Results show that the pulsatile VAD does not maintain the expected cardiac output at higher HR due to reduced SV. Data shown is the cohort mean across 6 patients.

Hemodynamics in an Abdominal Aortic Aneurysm: Multiscale Open-Loop *In Vitro* Model

Hemodynamic parameters such as the 3D blood flow and pressure fields have direct effects on the initiation and development of atherosclerosis and aneurysms (Taylor 1971; Glagov 1988; Ku 1985; Malek 1999). Modern imaging techniques such as phase-contrast magnetic resonance imaging can be used in an *in vitro* experiment to perform high-resolution direct measurements of flow velocity patterns in an anatomical phantom. In this case study, we demonstrate an *in vitro* model for studying the blood flow patterns in an abdominal aortic aneurysm (Kung 2011b).

A flow phantom made of MR-compatible resin (WaterShed® XC 11122, DSM Somos®, Elgin, IL) is 3D-printed according to a patient anatomical model constructed from a gadolinium-enhanced magnetic resonance angiography of the patient; anatomy of the abdominal aortic aneurysm and the renal and common iliac arteries are included in the flow phantom (Figure 13). Two RCR blocks are constructed to create downstream vascular impedances for the renal and aortic outlets of the phantom. The values of the resistor and capacitor components are set to produce physiologically realistic pressure and flow split waveforms under a physiologically realistic inlet flow waveform (Table 11.2). The resistor components are constructed by placing a large number of thin-walled glass capillary tubes (Sutter Instrument, CA) in parallel inside a plexiglass cylinder. The capacitor components have a smooth contour for the inlet in order to minimize flow turbulences and thus avoid parasitic resistances.

Table 11.1. Maximum cardiac output (L/min) achieved in each patient without VAD, with pulsatile VAD, and with continuous VAD

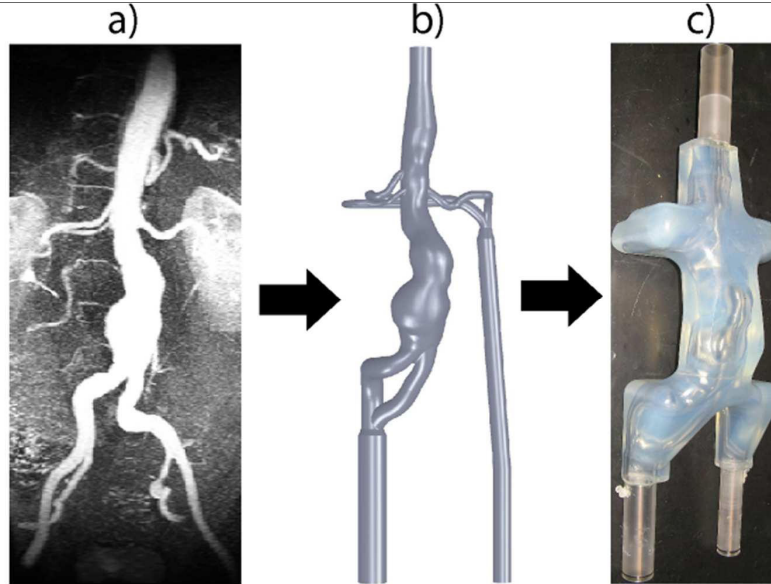|	Patient A	Patient B	Patient C	Patient D	Patient E	Patient F
Pre-VAD	1.29	1.55	1.42	1.60	1.87	1.75
Pulsatile VAD	1.92	2.30	2.14	2.24	2.21	2.79
Continuous VAD	3.11	3.37	3.36	3.51	3.31	4.09

Figure 13. Anatomical phantom construction: a) MR Imaging data from an abdominal aortic aneurysm patient. b) 3D computer model constructed based on patient imaging data. c) Physical phantom constructed from 3D computer model (Kung 2011b).
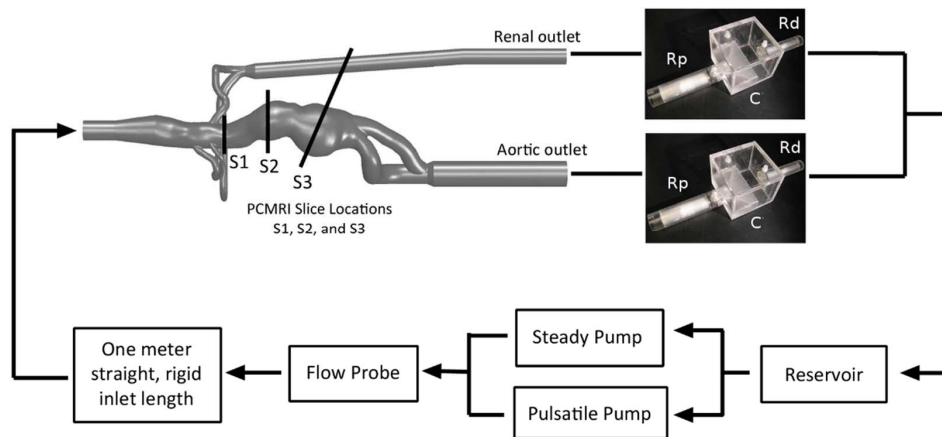

Figure 14. Flow system setup for the abdominal aortic aneurysm *in vitro* model.

Table 11.2. Values of lumped-parameter components in the RCR blocks of the abdominal aortic aneurysm *in vitro* model. Rp, C, and Rd are the proximal resistance, capacitance, and distal resistance, respectively

	Aortic outlet	Renal outlet
Rp (dynes-s/cm^5)	549	3053
C (cm^5/dynes)	3.25e-4	1.64e-4
Rd (dynes-s/cm^5)	7132	5951

We connect the RCR blocks to the anatomic flow phantom and place them in a flow system (Figure 14). Based on the flow waveforms measured in the patient (Bax 2005; Les 2010), we use a custom-built, MR-compatible, and computer-controlled pulsatile pump (Ku 2005) in parallel with a steady flow pump (Model 3-MD-HC, Little Giant Pump Co., OK) to reproduce the supra-renal aortic flow waveforms as the input flow to the phantom. The phantom input flow is monitored using a MR-compatible ultrasonic transit-time flow sensor (8PXL, Transonic Systems, NY).

Using a cardiac-gated 2D 3-component cine PCMRI sequence in a 1.5T GE MR scanner (Signa, GE Medical Systems, Waukesha, WI) and an 8-channel cardiac coil, we acquire flow velocity measurements at different slice locations within the phantom. The slice locations represent the mid-aneurysm location for each lobe of the bilobed aneurysm anatomy and the location directly downstream of the renal branches where flow is likely to be complex. As we examine the velocity imaging results at different time points in the flow cycle (Figure 15), it is easy to see the prominent swirling of blood and the stagnant regions in the large aneurysm. This observed flow pattern may provide information regarding the endothelial health in the aneurysm. Such an *in vitro* setup can also serve as a testbed to investigate the hemodynamic effects of various surgical procedures or vascular device implantations.

Virtual Surgery of the Superior Vena Cava to Pulmonary Artery Anastomosis: Multiscale Closed-Loop Computational Model

In this case study we demonstrate the use of a multiscale closed-loop computational model to predict and compare surgical outcomes of the single ventricle stage 2 palliation procedure. In this surgical procedure, the superior vena cava is connected to the pulmonary artery via two options: the "Glenn" or the "Hemi-Fontan" procedure (Norwood 1991). The Glenn procedure severs the superior vena cava from the right atrium and connects it to the right pulmonary artery, where the Hemi-Fontan procedure connects the top half of the right atrium to the pulmonary artery while leaving the superior vena cava attached to the atrium. Various degrees of left pulmonary stenosis are common among these patients, and part of the consideration of the stage 2 procedure is whether to perform the additional surgical steps to remove the stenosis, if present. Using a multiscale computational model, we investigate the hemodynamic differences between the Glenn and the Hemi-Fontan surgical options, as well as the physiologic impacts of a left pulmonary stenosis.
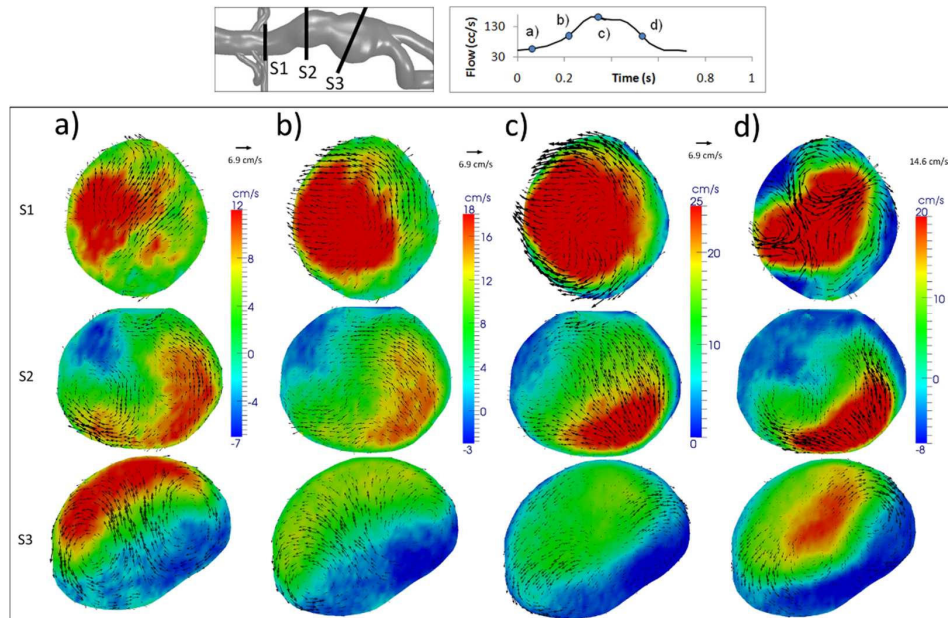

Figure 15. Phase-contrast magnetic resonance imaging measured flow velocities in the abdominal aortic aneurysm *in vitro* phantom experiment.
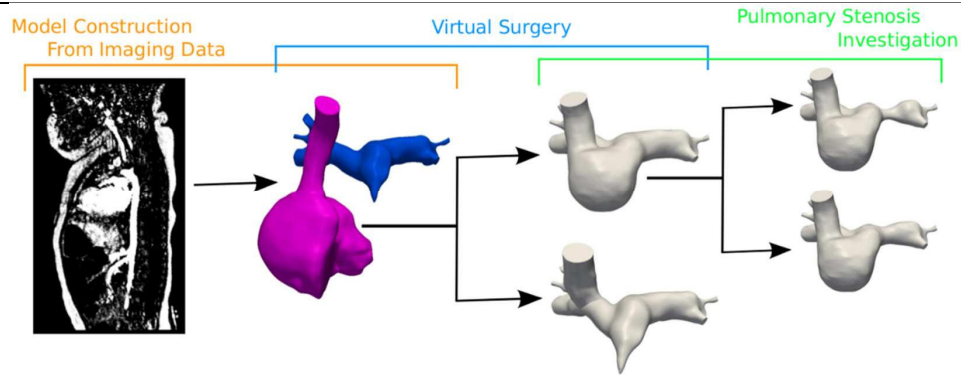
Figure 16. Virtual surgery and virtual pulmonary stenosis investigation from preoperative 3D anatomical model constructed based on patient imaging data. (Marsden 2015).
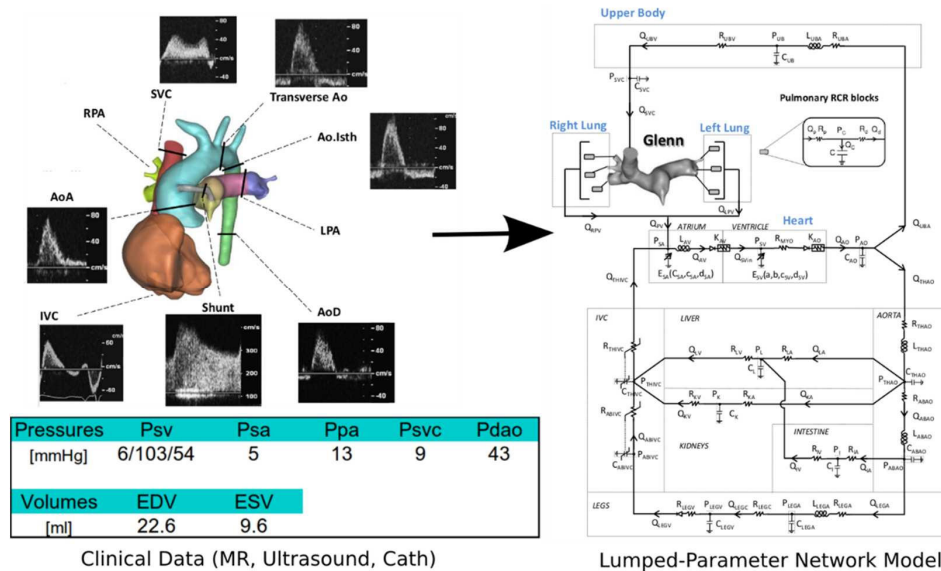

Figure 17. Preoperative clinical data supplies parameter tuning information for the closed-loop multiscale model consisting of a LPM coupled to a 3D anatomical model. (Marsden 2015).

From 3D imaging data of a patient, we construct a high-order computational model that is a representation of the patient's pre-operative anatomy. We then perform "virtual" Glenn or Hemi-Fontan surgeries and add a "virtual" left pulmonary stenosis of various severities by computationally modifying the pre-operative anatomic geometry (Figure 16). Using the pre-operative clinical data from the same patient, we tune an LPM (the low-order model) to represent the global circulation of the patient and couple the high and low order models to complete a multiscale simulation setup (Figure 17). The coupled multiscale simulation is run using open source software Simvascual (www.simtk.org) on a super computing cluster.
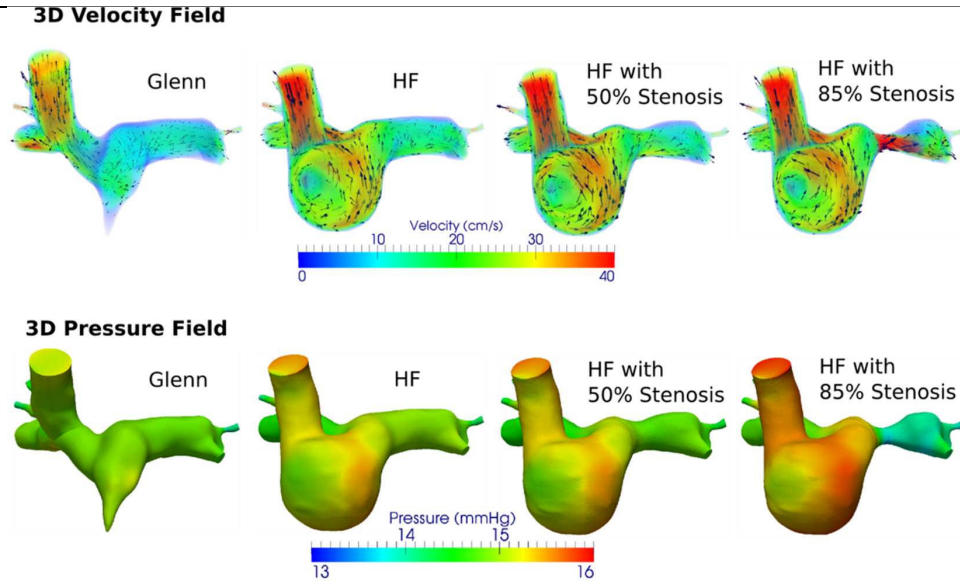
Figure 18. Simulated 3D pressure and flow patterns in the high-order model (Marsden 2015).
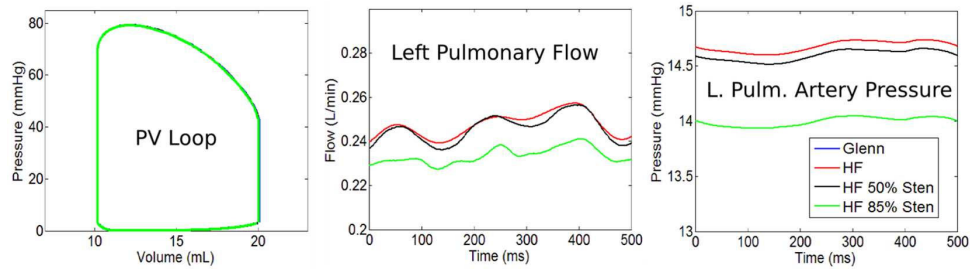

Figure 19. 0D physiologic parameters extracted from the low-order model (Marsden 2015).

Clinically relevant information such as the 3D pressure and flow in the high-order model (Figure 11.18), time tracings of physiologic parameters in the LPM (Figure 19), and power loss in the surgical junction relative to other systemic powers (Figure 20) can be extracted from the multiscale simulation results. This modeling investigation reveals that while flow patterns within the surgical junction are affected by different surgical options, physiology at the global level is not. In this particular case study, a 50% or 85% area stenosis also does not produce a significant impact to the global physiology. This is due to the fact that compared to the systemic power losses, the power loss in the surgical junction is relatively small. The differences in the 3D flow patterns between the surgical options, however, may provide information for assessing clinical considerations such as thrombotic risk.
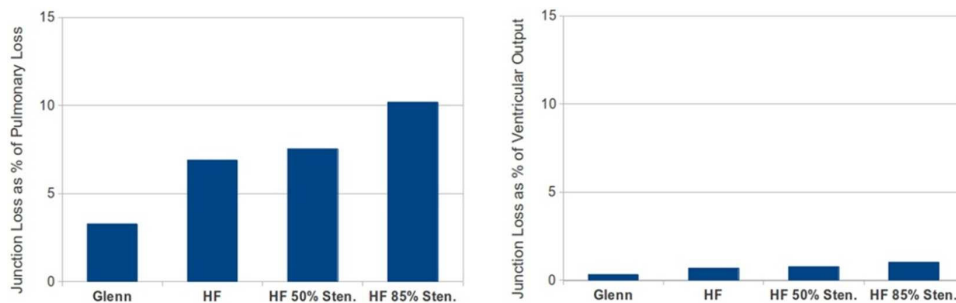

Figure 20. Power loss in the surgical junction as a fraction of other systemic powers (Marsden 2015).

MODEL SELECTION

Designing a cardiovascular model that is appropriate for the topic of study is essential for obtaining meaningful results. The choices between high versus low order models and computational versus *in vitro* models should depend on the input information available, the output information desired, and the aspects of biomechanics important to the study.

Low-Order versus High-Order

The main advantage of low-order models is that they are relatively low-cost to perform. Low-order models are suitable for simulating overall physiology and examining pressure and flow waveforms at different parts of the circulation. Since detailed geometric data is not required for model construction, it is also simpler (compared to high-order models) to create new implementations to describe complex scenarios such as the operation of active medical devices (i.e., the first example case study) as long as enough data is available to construct the required mathematical descriptions. The limitation of low-order models is their inability to account for or capture 3D parameters; therefore in the cases where the effects of these 3D quantities are important to the topic of study, high-order models should be employed. High-order models require detailed geometric input information and are labour-intensive to construct. Simulations of high-order models are also computationally expensive. In the choice between high or low order models, one should determine whether geometry or 3D dynamics affect the quantities of interest or whether the 3D parameters themselves are the quantities of interest. If the answer is yes to either of these questions, a high-order model is suitable. The use of high-order models should be limited to regions of the circulation that require them. The rest of the circulation should be represented using low-order models in order to achieve the most resource-efficient multiscale modeling approach for a research study.

Computational versus *In Vitro*

Computational models are typically less costly and quicker to construct than *in vitro* models. A computational low-order model can be set up within minutes with a few lines of code while an *in vitro* model could require hours of machining and physically connecting several components in a flow loop. In research studies that investigate systematic changes in a model, a computational setup can be automated to require minimal manual involvement. Extraction of output parameters is also more straight-forward in a computational model, as the desired information can be directly accessed from the computation data. In an *in vitro* model, measurements of the desired parameters require different sensor implementations and/or imaging setup and are subject to measurement noise and limited resolution. Measurements in an *in vitro* model with magnetic resonance, ultrasound, or particle imaging velocimetry often bring challenging technical requirements for phantom construction and experiment setup. For example, all of the devices in an *in vitro* setup for magnetic resonance imaging must be MR compatible to ensure safety and to avoid signal interference and imaging artifacts. This often means a large physical setup since long tubing and cables are required to keep the flow pump and pressure measurement equipment at a safe distance from the MR scanner. In an experiment for particle imaging velocimetry, index of refraction must be matched between the phantom and the working fluid, which significantly complicates phantom construction and often results in the necessity of adding corrosive chemicals such as sodium iodide in the working fluid. The strict geometrical setup criteria of particle imaging velocimetry also limit data acquisition to very few imaging planes. Lastly, the ability for *in vitro* models to describe the closed-loop response of the heart to changing preload and afterload is currently primitive, presenting a significant limitation compared to computational models.

On the other hand, computational models may not capture as many aspects of the relevant physics compared to *in vitro* models, especially in the area of fluid-structure interactions. Computational simulations of fluid-structure interactions are technically challenging, and reliable simulation techniques may not exist for the scenarios of interest. For example, current computational capabilities for simulating heart valve dynamics are primitive and very few groups have successfully performed simulations able to model leaflet contact (Wu 2016). Transient analysis of 3D computational models involving rotary blood pumps is extremely computationally expensive, therefore most studies are limited to steady-state analyses without accounting for realistic pulsatile flow scenarios (Fraser 2011). For the situations where computational methods face significant limitations, an *in vitro* model where the fluid-structure interactions are directly replicated in a physical setup may

be more suitable. *In vitro* high-order models are often suitable for medical device studies, since the device to be investigated can be implemented directly into the anatomical phantom under realistic flow and pressure conditions. Measurements of the resulting hemodynamics can reveal detailed 3D mechanical interactions between device operation and patient physiology and anatomy.

CONCLUSION AND FUTURE PERSPECTIVES

Computational and *in vitro* cardiovascular biomechanical models provide highly-controlled approaches for studying the cardiovascular system. This chapter provides an overview of several major types of models, the pros and cons of each, and a few examples of model application. The proper selection of high-order versus low-order and computational versus *in vitro* models for each research topic is important for capturing the relevant dynamics and minimizing resource usage. When employed properly, the types of biomechanical models presented in this chapter can bring significant progress to a research project at lower costs of resource and time compared to the use of animal models.

There are several areas of current development towards broadening the scope and usefulness of cardiovascular biomechanics models. The first is the incorporation of cellular biomechanics and biochemistry to capture the interactions and effects of biological responses at the microscale. Computationally, this would involve coupling cellular kinetics models with macroscale hemodynamic models (i.e., those presented in this chapter). Experimentally, tissue engineered constructs containing live cells can be implemented into an anatomical vascular simulator and allowed to directly interact with the macroscale hemodynamics. Second, there is a need for *in vitro* models to accurately capture closed-loop responses of the cardiovascular system, which is important for accounting for physiologic feedback and assessing physiologic impacts. A method to address this need is currently being developed in the author's research group and referred to as the "Physiology Simulation Coupled Experiment." This approach is similar to the hardware-in-the-loop concept commonly used in the aviation industry and couples a high-order *in vitro* model to a low-order computational physiology model. Finally, there is a pressing need for the validation of model predictions against clinical data. Due to the limitations in clinical data acquisition and lack of clinical database for modeling purposes, reliable large-scale validation of cardiovascular biomechanical models is rare. Close coordination between clinicians and engineers is essential for bridging this gap and bringing the much-needed validation to justify application of these biomechanical models towards clinical use.

REFERENCES

Adachi I, and Fraser CD. Mechanical circulatory support for infants and small children. *Semin. Thorac. Cardiovasc. Surg. Pediatr. Card. Surg. Annu.* 2011; 14(1): 38−44.

Baloa LA, Boston J R, and Antaki J F. Elastance-based control of a mock circulatory system. *Ann Biomed Eng,* 2001;29(3):244−51.

Baretta A, Corsini C, Marsden A L, Vignon-Clementel I E, Hsia TY, Dubini G, Migliavacca F, and Pennati G. (2012) Respiratory effects on hemodynamics in patient-specific CFD models of the Fontan circulation under exercise conditions. *European Journal of Mechanics-B/Fluids* 2012; 35:61−69.

Bax L, Bakker, CJ, Klein WM, Blanken N, Beutler JJ, and Mali WP. Renal blood flow measurements with use of phase-contrast magnetic resonance imaging: normal values and reproducibility. *J. Vasc. Interv. Radiol.* 2005; 16(6):807−14.

Bayer JD, Blake RC, Plank G, and Trayanova NA. A novel rule-based algorithm for assigning myocardial fiber orientation to computational heart models. *Ann. Biomed. Eng.* 2012; 40(10) :2243−54.

Bazilevs Y, Hsu MC, Zhang Y, Wang W, Kvamsdal T, Hentschel S, and Isaksen JG. Computational vascular fluid-structure interaction: methodology and application to cerebral aneurysms. *Biomech. Model. Mechanobiol.* 2010; 9(4):481−98.

Borazjani I. Fluid–structure interaction, immersed boundary-finite element method simulations of bio-prosthetic heart valves. *Computer Methods in Applied Mechanics and Engineering* 2013; 257: 103−116.

Calvaruso DF, Ocello S, Salviato N, Guardì D, Petruccelli DF, Rubino A, Fattouch K, Cipriani A, and Marcelletti CF. Implantation of a Berlin Heart as single ventricle by-pass on Fontan circulation in univentricular heart failure. *ASAIO J.* 2007; 53(6): e1−2.

Cardarelli MG, Salim M, Love J, Simone S, Tumulty J, Conway D, and Griffith B. Berlin heart as a bridge to recovery for a failing Fontan. *Ann. Thorac. Surg.* 2009; 87(3):943−6.

Caro CG, Fitz-Gerald JM, and Schroter RC. Atheroma and arterial wall shear. Observation, correlation and proposal of a shear dependent mass transfer mechanism for atherogenesis. *Proc. R. Soc. Lond. B. Biol. Sci.* 1971;177(46) :109−59.

Cheng A, Williamitis CA, and Slaughter MS. Comparison of continuous-flow and pulsatile-flow left ventricular assist devices: is there an advantage to pulsatility? *Ann. Cardiothorac. Surg.* 2014; 3(6):573−81.

Chu MW, Sharma K, Tchervenkov CI, Jutras LF, Lavoie J, Shemie, SD, Laliberte E, Calaritis C, and Cecere R. Berlin Heart ventricular assist device in a child with hypoplastic left heart syndrome,' *Ann. Thorac. Surg.* 2007; 83(3):1179−81.

Corsini C, Baker C, Kung E, Schievano S, Arbia G, Baretta A, Biglino G, Migliavacca F, Dubini G, Pennati G, Marsden A, Vignon-Clementel I, Taylor A, Hsia TY, Dorfman A, and MOCHA Investigators. An integrated approach to patient-specific predictive modeling for single ventricle heart palliation. *Comput Methods Biomech Biomed Engin.* 2014;17(14):1572–89.

Drews T, Jurmann M, Michael D, Miralem P, Weng Y, and Hetzer R. Differences in pulsatile and non-pulsatile mechanical circulatory support in long-term use,' *J. Heart Lung Transplant.* 2008; 27(10):1096−101.

Feller ED, Sorensen EN, Haddad M, Pierson RN, Johnson FL, Brown JM, and Griffith BP. Clinical outcomes are similar in pulsatile and nonpulsatile left ventricular assist device recipients. *Ann. Thorac. Surg.* 83(3): 1082−8.

Ferrari G, De Lazzari C, Mimmo R, Tosti G, Ambrosi D, and Gorczynska K. A computer controlled mock circulatory system for mono- and biventricular assist device testing. *Int. J. Artif. Organs.* 1998;21(1): 26−36.

Figliola RS, Giardini A, Conover T, Camp TA, Biglino G, Chiulli J, and Hsia TY. In Vitro Simulation and Validation of the Circulation with Congenital Heart Defects. *Prog. Pediatr. Cardiol.* 2010; 30(1−2): 71−80.

Figueroa CA, Vignon-Clementel IE, Jansen KE, Hughes TJR, and Taylor CA. A coupled momentum method for modeling blood flow in three-dimensional deformable arteries. *Computer Methods in Applied Mechanics and Engineering* 2006;195(41−43): 5685−5706.

Fraser KH, Taskin ME, Griffith BP, and Wu ZJ. The use of computational fluid dynamics in the development of ventricular assist devices. *Med. Eng. Phys.* 2011;33(3):263−80.

Gijsen FJ, van de Vosse, FN, and Janssen JD. The influence of the non-Newtonian properties of blood on the flow in large arteries: steady flow in a carotid bifurcation model. *J. Biomech.* 1999;32(6):601−8.

Giridharan GA, Skliar M, Olsen DB, and Pantalos GM. Modeling and control of a brushless DC axial flow ventricular assist device. *ASAIO journal* 2002; 48(3): 272−289.

Glagov S, Zarins C, Giddens DP, and Ku DN. Hemodynamics and atherosclerosis. Insights and perspectives gained from studies of human arteries. *Arch. Pathol. Lab. Med.* 1988;112(10): 1018−31.

Gregory SD, Stevens M, Timms D, and Pearcy M. Replication of the Frank-Starling response in a mock circulation loop. *Conf. Proc. IEEE Eng. Med. Biol. Soc.* 2011:6825−8.

Griffith BE. Immersed boundary model of aortic heart valve dynamics with physiological driving and loading conditions. *Int. J. Numer. Method. Biomed. Eng.* 2012;28(3):317−45.

Groves EM, Falahatpisheh A, Su JL, and Kheradvar A. The effects of positioning of transcatheter aortic valves on fluid dynamics of the aortic root. *ASAIO.* 2014; 60(5):545−52.

Gwak KW, Noh MD, Paden BE, and Antaki J F. Fluidic operational amplifier for mock circulatory systems-simulation and experimental results. *Proceedings of the 2005. American Control Conference,* 2005; IEEE. 2005; 3817−3822.

Hetzer R, Potapov EV, Stiller B, Weng Y, Hübler M, Lemmer J, Alexi-Meskishvili V, Redlin M, Merkle F, Kaufmann F, and Hennig E. Improvement in survival after mechanical circulatory support with pneumatic pulsatile ventricular assist devices in pediatric patients. *Ann. Thorac. Surg.* 2006; 82(3): 917−24; discussion 924−5.

Hughes TJ, and Lubliner J. On the one-dimensional theory of blood flow in the larger vessels,' *Mathematical Biosciences,* 1973; 18(1):161−170.

Kato TS, Chokshi A, Singh P, Khawaja T, Cheema F, Akashi H, Shahzad K, Iwata S, Homma S, Takayama H, Naka Y, Jorde U, Farr M, Mancini DM, and Schulze PC. Effects of continuous-flow versus pulsatile-flow left ventricular assist devices on myocardial unloading and remodeling. *Circ. Heart Fail.* 2011; 4(5):546−53.

Khoiy KA, Biswas D, Decker TN, Asgarian KT, Loth F, and Amini R. Surface Strains of Porcine Tricuspid Valve Septal Leaflets Measured in Ex-vivo Beating Hearts. *Journal of Biomechanical Engineering.* 2016;138(11):111006.

Klotz S, Deng MC, Stypmann J, Roetker J, Wilhelm MJ, Hammel D, Scheld HH, and Schmid C. Left ventricular pressure and volume unloading during pulsatile versus nonpulsatile left ventricular assist device support. *Ann. Thorac. Surg.* 2004;77(1):143-9; discussion 149−50.

Krause E. Computational fluid dynamics: its present status and future direction. *Computers & fluids* 1985; 13(3):239−269.

Ku DN, Giddens DP, Zarins CK, and Glagov S. Pulsatile flow and atherosclerosis in the human carotid bifurcation. Positive correlation between plaque location and low oscillating shear stress. *Arteriosclerosis* 1985:5(3):293−302.

Ku JP, Elkins CJ, and Taylor CA. Comparison of CFD and MRI flow and velocities in an in vitro large artery bypass graft model. *Ann. Biomed. Eng.* 2005;33(3): 257−69.

Kung E, Baretta A, Baker C, Arbia G, Biglino G, Corsini C, Schievano S, Vignon-Clementel IE, Dubini G, Pennati G, Taylor A, Dorfman A, Hlavacek AM, Marsden AL, Hsia TY, and Migliavacca F. Predictive modeling of the virtual Hemi-Fontan operation for second stage single ventricle palliation: Two patient-specific cases. *Journal of Biomechanics* 2013; 46(2):423−9.

Kung E, Les A, Figueroa, CA, Medina F, Arcaute K, Wicker R., McConnell M, and Taylor C. In Vitro Validation of Finite Element Analysis of Blood Flow in Deformable Models. *Ann. Biomed. Eng.* 2011a; 39(7): 1947−60.

Kung E, Pennati G, Migliavacca F, Hsia TY, Figliola RS, Marsden A, Giardini A, and MOCHA Investigators. A Simulation Protocol For Exercise Physiology In Fontan Patients Using A Closed-Loop Lumped-Parameter Model,' *J. Biomech. Eng.* 2014; 136(8):81007.

Kung E, and Taylor C. Development of a Physical Windkessel Module to Re-Create In Vivo Vascular Flow Impedance for In Vitro Experiments. *Cardiovascular Engineering and Technology* 2011; 2(1):2−14.

Kung EO, Les AS, Medina F, Wicker RB, McConnell MV, and Taylor CA. In vitro validation of finite-element model of AAA hemodynamics incorporating realistic outlet boundary conditions. *J. Biomech. Eng.* 2011b; 133(4):041003.

Kung E, Perry JC, Davis C, Migliavacca F, Pennati G, Giardini A, Hsia TY, and Marsden A. Computational Modeling of Pathophysiologic Responses to Exercise in Fontan Patients. *Ann. of Biomed. Eng.* 2015; 43:1335–1347.

Langille BL, Bendeck MP, and Keeley FW. Adaptations of carotid arteries of young and mature rabbits to reduced carotid blood flow. *Am. J. Physiol.* 1989; 256(4 Pt 2):H931−9.

Lee J, Moghadam ME, Kung E, Cao H, Beebe T, Miller Y, Roman BL, Lien CL, Chi NC, and Marsden AL. Moving Domain Computational Fluid Dynamics to Interface with an Embryonic Model of Cardiac Morphogenesis. *PloS One* 2013;8(8): e72924.

Les AS, Shadden SC, Figueroa CA, Park JM, Tedesco MM, Herfkens RJ, Dalman RL, and Taylor CA. Quantification of hemodynamics in abdominal aortic aneurysms during rest and exercise using magnetic resonance imaging and computational fluid dynamics. *Ann. Biomed. Eng.* 2010;38(4):1288−1313.

Long CC, Hsu MC, Bazilevs Y, Feinstein JA, and Marsden AL. Fluid-structure interaction simulations of the Fontan procedure using variable wall properties. *Int. J. Numer. Method Biomed. Eng.* 2012; 28(5):513−27.

Malek AM, Alper SL, and Izumo S. Hemodynamic shear stress and its role in atherosclerosis. *JAMA* 1999; 282(21):2035−42.

Marsden A, and Kung E. Multiscale Modeling of Cardiovascular Flows,' *Computational Bioengineering*: CRC Press 2015:163−190.

Mechoor RR, Schmidt T, and Kung E. A Real-Time Programmable Pulsatile Flow Pump For In-Vitro Cardiovascular Experimentation *Journal of Biomechanical Engineering*. 2016;138(11):111002.

Migliavacca F, Dubini G, Pennati G, Pietrabissa R, Fumero R, Hsia TY, and de Leval MR. Computational model of the fluid dynamics in systemic-to-pulmonary shunts. *J. Biomech.* 2000;33(5):549−57.

Milner JS, Moore JA, Rutt BK, and Steinman DA. Hemodynamics of human carotid artery bifurcations: computational studies with models reconstructed from magnetic resonance imaging of normal subjects. *J. Vasc. Surg.* 1998; 28(1):143−56.

Moazami N, Fukamachi K, Kobayashi M, Smedira NG, Hoercher KJ, Massiello A, Lee S, Horvath DJ, and Starling RC. Axial and centrifugal continuous-flow rotary pumps: a translation from pump mechanics to clinical practice. *J. Heart Lung Transplant* 2013; 32(1): 1−11.

Norwood JWI. Hypoplastic left heart syndrome. *The Annals of Thoracic Surgery* 1991; 52(3):688−695.

Pahlevan NM, and Gharib M. In-vitro investigation of a potential wave pumping effect in human aorta. *J. Biomech.* 2013;46(13):2122−9.

Pantalos GM, Koenig SC, Gillars KJ, Giridharan GA, and Ewert DL. Characterization of an adult mock circulation for testing cardiac support devices. *ASAIO J.* 2004; 50(1):37−46.

Pekkan K, Frakes D, De Zelicourt D, Lucas CW, Parks WJ and Yoganathan AP. Coupling pediatric ventricle assist devices to the Fontan circulation: simulations with a lumped-parameter model. *ASAIO J.* 2005; 51(5): 618−28.

Peskin CS. Flow patterns around heart valves: a numerical method. *Journal of computational physics* 1972;10(2) :252−271.

Salamonsen RF, Lim E, Moloney J, Lovell NH, and Rosenfeldt FL. Anatomy and Physiology of Left Ventricular Suction Induced by Rotary Blood Pumps. *Artif. Organs* 2015; 39(8):681−90.

Schiavazzi DE, Kung EO, Marsden AL, Baker C, Pennati G, Hsia TY, Hlavacek A, Dorfman AL, and MOCHA Investigators. Hemodynamic effects of left pulmonary artery stenosis after superior cavopulmonary connection: A patient-specific multiscale modeling study,' *J. Thorac. Cardiovasc. Surg.* 2015; 149(3):689−696.e3.

Schmidt T, Rosenthal D, Reinhartz O, Riemer K, He F, Hsia TY, Marsden A, Kung E. and MOCHA Investigators. Superior performance of continuous over pulsatile flow ventricular assist devices in the single ventricle circulation: A computational study. *J. Biomech.* 2016; 52: 48−54.

Soler L, Delingette H, Malandain G, Montagnat J, Ayache N, Koehl C, Dourthe O, Malassagne B, Smith M, Mutter D, and Marescaux J. Fully automatic anatomical, pathological, and functional segmentation from CT scans for hepatic surgery. *Comput. Aided. Surg.* 2001; 6(3):131−42.

Steinman DA. Image-based computational fluid dynamics modeling in realistic arterial geometries. *Ann. Biomed. Eng.* 2002; 30(4):483−97.

Stiller B, Hetzer R, Weng Y, Hummel M, Hennig E, Nagdyman N, Ewert P, Lehmkuhl H, and Lange PE. Heart transplantation inhildren after mechanical circulatory support with pulsatile pneumatic assist device. *J. Heart Lung Transplant.* 2003;22(11):1201−8.

Suga H, Sagawa K, and Shoukas AA. Load independence of the instantaneous pressure-volume ratio of the canine left ventricle and effects of epinephrine and heart rate on the ratio. *Circulation Research* 1973;32(3): 314−322.

Taylor C, Hughes T, and Zarins C. Finite element modeling of blood flow in arteries. *Computer Methods in Applied Mechanics and Engineering,* 1998a;158(1−2):155−196.

Taylor C, and Steinman D. Image-Based Modeling of Blood Flow and Vessel Wall Dynamics: Applications, Methods and Future Directions: Sixth International Bio-Fluid Mechanics Symposium and Workshop, March 28−30, 2008, Pasadena, California (Position Paper), *Annals of Biomedical Engineering* 2008; 38(3):1188−1203.

Taylor CA, Draney MT, Ku JP, Parker D, Steele BN, Wang K, and Zarins CK. Predictive medicine: computational techniques in therapeutic decision-making. *Comput. Aided Sur.* 1999; 4(5):231−47.

Taylor CA, Hughes TJ, and Zarins CK. Finite element modeling of three-dimensional pulsatile flow in the abdominal aorta: relevance to atherosclerosis. *Ann. Biomed. Eng.* 1998b;26(6): 975−87.

Thiry PS, and Roberge FA. Analogs and models of systemic arterial circulation. *Rev. Can. Biol.* 1976; 35(4):217−38.

Timms DL, Gregory SD, Greatrex NA, Pearcy MJ, Fraser JF, and Steinseifer U. A compact mock circulation loop for the in vitro testing of cardiovascular devices. *Artif. Organs* 1976; 35(4):384−91.

Trayanova NA. Whole-heart modeling: applications to cardiac electrophysiology and electromechanics. *Circ. Res.* 2011; 108(1):113−28.

Vukicevic M, Chiulli JA, Conover T, Pennati G, Hsia TY, Figliola RS, and Network M. Mock circulatory system of the Fontan circulation to study respiration effects on venous flow behavior. *ASAIO J.* 2013; 59(3):253−60.

Watton PN, Luo XY, Wang X, Bernacca GM, Molloy P, and Wheatley DJ. Dynamic modelling of prosthetic chorded mitral valves using the immersed boundary method. *J. Biomech.* 2007; 40(3):613−26.

Westerhof N, Bosman F, De Vries CJ, and Noordergraaf A. Analog studies of the human systemic arterial tree. *J. Biomech.* 1969;2(2):121−43.

Westerhof N, Lankhaar JW, and Westerhof BE. The arterial Windkessel. *Med. Biol. Eng. Comput.* 2009; 47(2):131−41.

Wolinsky H. and Glagov S. A lamellar unit of aortic medial structure and function in mammals. *Circ. Res.* 1967; 20(1), :99-111.

Wu W, Pott D, Mazza B, Sironi T, Dordoni E, Chiastra C, Petrini L, Pennati G, Dubini G, Steinseifer U, Sonntag S, Kuetting M, and Migliavacca F. Fluid-Structure Interaction Model of a Percutaneous Aortic Valve: Comparison with an In Vitro Test and Feasibility Study in a Patient-Specific Case. *Ann. Biomed. Eng.* 2016;44(2):590−603.

Zheng X, Seo J, Vedula V, Abraham T, and Mittal R. Computational modeling and analysis of intracardiac flows in simple models of the left ventricle. *European Journal of Mechanics-B/Fluids.* 2012; 35:31−39.